Journal of Molecular Catalysis A: Chemical 326 (2010) 29–40

Contents lists available at ScienceDirect

Journal of Molecular Catalysis A: Chemical

journal homepage: www.elsevier.com/locate/molcata

Review

Study of bimetallic interactions and promoter effects of FeZn, FeMn and FeCr Fischer–Tropsch synthesis catalysts

Hulin Wang[a,b,c], Yong Yang[a,b,*], Jian Xu[a], Hong Wang[a,b], Mingyue Ding[a,b], Yongwang Li[a,b]

[a] National Engineering Laboratory for Indirect Coal Liquefaction, Institute of Coal Chemistry, Chinese Academy of Sciences, Taiyuan 030001, People's Republic of China
[b] State Key Laboratory of Coal Conversion, Institute of Coal Chemistry, Chinese Academy of Sciences, Taiyuan 030001, People's Republic of China
[c] Graduate School of the Chinese Academy of Sciences, Beijing 100039, People's Republic of China

ARTICLE INFO

Article history:
Received 18 December 2009
Received in revised form 18 April 2010
Accepted 20 April 2010
Available online 28 April 2010

Keywords:
Fischer–Tropsch synthesis
Zn promotion
Cr promotion
Mn promotion
Fe-based catalyst

ABSTRACT

The promotional effects of transition metals of Zn, Mn and Cr on the textural properties, reduction behavior, surface basicity, structural changes during reduction and reaction, and the catalytic performances of Fe-based Fischer–Tropsch synthesis (FTS) catalysts were investigated by N_2 physisorption, X-ray diffraction (XRD), Mössbauer spectroscopy (MES), extended X-ray absorption fine structure (EXAFS), X-ray photoelectron spectroscopy (XPS), CO temperature-programmed reduction (CO-TPR), H_2-differential thermogravimetric analysis (H_2-DTG) and CO_2 temperature-programmed desorption (CO_2-TPD). The FTS reaction behaviors of the catalysts were measured at 1.5 MPa, 260 °C and syngas with H_2/CO ratio of 2.0. The results show that there are two distinct forms of bimetallic interactions for the promoted catalysts, namely (1) $ZnFe_2O_4$ compound formed for Zn-promoted iron catalyst and (2) solid solutions observed for those promoted by either Cr or Mn promoters. The presence of $ZnFe_2O_4$ compound in the Zn-promoted catalyst leads to the phase separations between Zn and Fe oxides, and therefore very similar catalytic behavior to that of unpromoted catalyst. The stability of activity was improved due to the increased dispersion of active site through the formation of $ZnFe_2O_4$ compound. In contrast, for the Mn- and Cr-promoted catalysts, the solid solutions in FeMn and FeCr systems strongly inhibit the reduction of the catalysts, and enhance the stability of catalytic activity. The FTS tests show that Mn and Cr promoters enhance the olefin and C_{5+} hydrocarbon selectivity and restrain the methane selectivity due to their more strong basic sites. Besides the surface basicity the selectivities of Mn-promoted catalyst are also correlated with the enrichment of Mn on the catalyst surface.

Contents

* Corresponding author at: National Engineering Laboratory for Indirect Coal Liquefaction, Institute of Coal Chemistry, Chinese Academy of Sciences, Taiyuan 030001, People's Republic of China. Tel.: +86 351 7560835; fax: +86 351 7560835.
E-mail address: yyong@sxicc.ac.cn (Y. Yang).

1381-1169/$ – see front matter © 2010 Elsevier B.V. All rights reserved.
doi:10.1016/j.molcata.2010.04.009

1. Introduction

Fischer–Tropsch synthesis (FTS) is an important route for converting syngas, a mixture of CO and H_2, derived from natural gas, coal and biomass to liquid fuels and other chemicals, in which Fe and Co catalysts have been commercially used. Fe-based FTS catalyst is favored due to its low cost, adjustable selectivity, and reasonable water–gas shift (WGS) activity which means a flexible operation for the industrial process [1–3]. Commercial FTS Fe catalyst, mainly composed of Fe oxide, is often promoted with transition metal oxides, alkali salts and structural promoters to improve its physico-chemical performances.

Alkali promoter, such as potassium, is added mainly to enhance the dissociative adsorption of CO, which subsequently could improve the carburization and suppress the methane formation of the catalyst. At the same time, structure promoters, often SiO_2 or/and Al_2O_3, are added to improve the structural stability of the catalyst [1–5].

Additionally, transition metal promoters such as Cu, Mn, Cr, Zn, Ni and Mo are also incorporated into Fe-based FTS catalyst to optimize the chemical environment of the catalyst. Among them, Cu is widely used in commercial FTS process, since the presence of Cu facilitates the reduction of α-Fe_2O_3 to Fe_3O_4 or metallic Fe [1,6–8]. Ni promoter is seldom used in FTS catalyst due to the high selectivity to methane. Whereas the addition of Mo to iron FTS catalyst would form too strong interaction of Fe–O–Mo to inhabit the reduction and carburization of iron oxide and decrease the catalytic activity [9].

Unlike the above-mentioned Ni and Mo promoters, the addition of Mn, Cr and Zn promoters shows favorable effects on iron FTS catalysts, but their effects are still in controversial. Mn promoter is generally proved that it could not only stabilize the catalytic activity, but also enhance the light olefin selectivity and decrease the selectivity to methane for the iron FTS catalyst [10–14]. However, these promotions were not proved by Satterfield and Stenger's work [15]. Cr promoter was reported to enhance the selectivity of heavy hydrocarbon products for precipitated Fe catalyst [16]. However, it is generally used as a promoter for WGS reaction, which would lead to a high H_2/CO ratio in FTS process and are benefit for the production of light hydrocarbon [17,18]. Zn was found to increase the FTS activity over a precipitated Fe–Cu–Zn–K catalyst with optimized Zn/Fe ratio of 0.1 and have no influence on the product selectivity [8,19,20]. While Zn was also reported that it could improve the olefin selectivity over a FeZn ultrafine particle catalyst [21]. The main reasons for these different results on the promotion of the transition promoters (M) are probably caused by the complexity of the catalytic system in which there are too many interactions between promoters and iron, such as Fe–M, Fe–Si, Fe–K and Fe–Cu, etc. [6]. It is difficult to discern the inherent promotion of the transition metals for the iron FTS catalyst incorporated with other chemical and structural promoters.

In the present study, the promotions of transitional metals (M) of Zn, Mn and Cr were investigated over bimetallic FeM catalyst system without any other promoter being added, which could shield the effect of other interaction and present only the promotion of transition metals. The catalytic performance was investigated in a fixed bed reactor and the fresh, reduced, and used catalysts were systematically characterized. The catalytic activities and selectivities for hydrocarbon products are compared to the unpromoted α-Fe_2O_3 to illustrate the effects of transition metals on the Fe FTS catalysts.

2. Experimental

2.1. Catalyst preparation

The catalysts used in the present study were prepared by using the continuous coprecipitation. A salt solution containing both $Fe(NO_3)_3$ and $M(NO_3)_x$ (M = Zn, Mn and Cr) and a separate solution of $NH_3{\cdot}H_2O$ were used in the precipitation processes. The salt solution and ammonia solution were preheated to 85 °C and 40 °C, respectively. Under stirring, the salt solution (flow rate 60 ml/min) and $NH_3{\cdot}H_2O$ solution were added into a continuously stirred tank reactor for the precipitation with pH 8.2–8.5, in which the dropping rate of ammonia solution was adjusted to keep the constant pH value of the mixture. The temperature of the precipitation unit was kept at 80 °C during the whole precipitation process. The precipitate was washed thoroughly with deionized water and filtered subsequently. The final cake was reslurried in deionized water and spray dried in air at 250 °C. The atomic ratio of iron to promoters is designed to 100:5, named C-05, M-05 and Z-05 for Cr, Mn and Zn, respectively. The catalyst samples were then calcinated at 550 °C for 5 h. The benchmark catalyst α-Fe_2O_3 and reference compounds (ZnO, Mn_2O_3 and Cr_2O_3) were obtained by precipitated nitrates of metals as the method described above. In all tests, the catalysts were pressed into pellets, crushed and sieved to retain 20-40 mesh particles prior to loading to a fixed bed reactor.

2.2. Catalyst characterizations

The BET surface area, pore volume and average pore diameter of the fresh catalysts were measured with the nitrogen physisorption at −196 °C in ASAP 2420 (Micromeritics, USA). Each sample was degassed under vacuum at 90 °C for 1 h and 350 °C for 8 h prior to the measurement.

Powder X-ray diffraction (XRD) measurements were carried out using a D/max-RA X-ray diffractometer (Rigaku, Japan) with Cu Kα radiation (λ = 0.154 nm) operated at 40 kV and 100 mA. The crystal phase compositions of the samples were determined by comparing the measured d-spacings with standard ASTM values. Silicon was used as an internal standard for correction of the angles derived from the diffraction lines and of the instrumental broadening for the crystallite size and cell parameters determination.

The Mössbauer effect spectroscopy (MES) experiments were carried out in a CANBERRA series 40 MCA constant-acceleration drive with a triangular reference signal at room temperature. The radioactive source was a 25 mCi ^{57}Co in Pd matrix.

The spectra were analyzed by a non-linear least square fitting procedure.

The X-ray absorption spectra at Fe, Mn, Cr and Zn K-edge for the as-prepared catalysts and the reference compounds were measured at the beamline of U7C of National Synchrotron Radiation Laboratory (NSRL) and 4W1B of Beijing Synchrotron Radiation Facility (BSRF). The storage ring of NSRL and BSRF were operated at 0.8 GeV with a maximum current of 160 mA and 2.2 GeV with a maximum current of 100 mA, respectively. The fixed-exit Si (1 1 1) flat double crystals were used as monochromators. The EXAFS at K-edge of the metals were collected in transmission mode. EXAFS data were analyzed by a NSRL XAFS 3.0 data analysis package compiled by Zhong and Wei according to the standard procedures [22,23].

XPS spectra were taken by a VG MiltiLab 2000 system with Al Kα (1486.6 eV) as the X-ray source. The C 1s as a reference signal was adjusted to 284.6 eV. High-resolution spectral envelopes were obtained by curve fitting synthetic peak components using the XPS peak software. The raw data were used with no preliminary smoothing. Symmetric Gaussian–Lorentzian product functions were used to approximate the line shapes of the fitting components.

The CO temperature-programmed reduction (CO-TPR) was carried out using a chemisorption analyzer (Micromeritics, Model 2920) over 30 mg sample with 50 ml/min reducing gas composed of 10% CO (by mole basis) mixed with He. The reactor was heated from room temperature to 800 °C at a heating rate of 10 °C/min. Prior to TPR, the samples was treated under 50 ml/min He at 500 °C for 1 h.

The H_2-differential thermogravimetric analysis (H_2-DTG) was performed using a TGA92 thermogravimetric system (Setaram, France) with a flow of 10% H_2 in Ar as the reduction gas. Typically, 20–30 mg samples were treated in 10% H_2–Ar and then temperature was increased from room temperature to 800 °C at a rate of 10 °C/min and held for 5 min before cooling.

The CO_2-TPD experiments were performed in the same system as used in CO-TPR with He as carrier gas. About 300 mg sample was loaded in the reactor and purged with He (50 ml/min) and calcined in situ at 500 °C for 1 h to remove the adsorption species from the catalysts. In the following steps, CO_2 adsorption on catalyst was performed at 50 °C for 30 min, and then the sample was purged with the carrier gas for 30 min to remove the weakly adsorbed species. After this step, temperature was increased to 500 °C at a rate of 10 °C/min.

2.3. Fischer–Tropsch reaction

A detailed description of the reactor and the product collection system was given by Ji et al. [24]. Briefly, experiments were conducted in a 12-mm i.d. stainless steel fixed bed reactor, and the feed gas with a H_2/CO ratio of approximately 2.0 go through a series of columns, an activated charcoal trap, an oxygen-removal trap, a sulfur-removal trap and a silica gel/5A molecular sieve trap, to remove tiny amounts of carbonyls, oxygen, sulfur and water before it enters the reactor. The flow rate of the purified syngas was controlled by using a mass flow controller 5850E (Brooks, USA). The outlet of the reactor is connected with a hot trap (120 °C) and a cold trap (0 °C) at the system pressure. After the product collectors, the pressure of the tail gas was released through a backpressure regulator (Swagelok, USA). The flow rate of tail gas was monitored by a wet-gas flow meter. Typically, for all reaction experiments, 4 g catalyst was charged in the reactor. The remaining volume of the reactor tube was filled with ceramics beads in a diameter range of 10–20 mesh. Before reaction, all catalysts were reduced with syngas (H_2/CO = 2.0) at 280 °C, 0.10 MPa and 1000 ml/(g h) for 24 h. Following activation, the bed was cooled to 200 °C. The system was then pressurized to 1.50 MPa. The temperature was gradually increased to 280 °C. After this unsteady state period, the products in the hot and cold traps are collected over 24 h (mass balance period), weighted, and sampled for analysis. The tail gas was analyzed online by gas chromatography (GC) 6890N and 4890D (Agilent, USA). The liquid sample was withdrawn every 24 h and analyzed on an off-line GC 6890N (Agilent, USA).

The reduced catalyst samples used for XRD and MES characterization were prepared by reducing the fresh catalysts in the fixed bed reactor with syngas (H_2/CO = 2) at 280 °C, 0.10 MPa and 1000 ml/(g h) for 24 h. After reduction, the reactor was cooled to room temperature and then extensively purged with N_2 in which minimum O_2 was present for passivation. Finally the catalysts were coated with paraffin wax for preventing the oxidation and then sealed for characterization.

3. Results

3.1. Textural properties of the fresh catalysts

Textural properties and pore size distributions of the fresh catalyst with different promoters are shown in Table 1. As shown in Table 1, the BET surface areas of all catalysts are low (18–31 m^2/g) due to the absence of SiO_2 [3]. With the additions of Zn, Mn and Cr promoters, it can be observed that the BET surface area increases from 18 m^3/g to 20 m^3/g, 27 m^3/g, 31 m^3/g, respectively. At the same time, the average of pore size decreases gradually for promoted catalysts to 37.7 nm, 35.7 nm and 27.8 nm, respectively. Additionally, the pore size distribution of the catalysts (see Supplementary information, Fig. S1) undergoes a slight shift towards small pore size with the addition of Zn, Mn and Cr. Furthermore, the addition of promoters in catalysts also affects the crystallite size for α-Fe_2O_3 phase. It can be seen that the crystallite size for α-Fe_2O_3 phase decreases from 31.5 nm for unpromoted catalyst to 30.9 nm, 26.6 nm and 25.0 nm for Zn-, Mn- and Cr-promoted catalysts, respectively.

3.2. Surface composition of fresh catalysts

XPS spectra of the Cr 2p, Mn 2p and Zn 2p core levels of the fresh samples were collected (Fig. 1). The surface compositions of the catalyst calculated from the analysis of these spectra are presented in Table 2. It is found that the surface M/Fe atomic ratio (M = Cr, Mn, Zn) is much larger than that in the bulk of the samples due to the enrichment of promoters on the surface of the catalysts.

Table 1
The textural properties of the as-prepared catalysts.

Catalysts	Analyzed composition (by atomic ratio)	BET surface area (m^2/g)	Pore volume (cm^3/g)	Average pore size (nm)	Crystallite size[a] (nm)
α-Fe_2O_3	–	18	0.14	31.5	31.5
Z-05	100Fe/5.5Zn	20	0.20	27.8	30.9, 12.8[b]
M-05	100Fe/4.8Mn	27	0.29	35.7	26.6
C-05	100Fe/5.1Cr	31	0.24	37.7	25.0

[a] Calculated from the Debye–Scherrer equation for hematite Fe_2O_3.
[b] Calculated for $ZnFe_2O_4$.

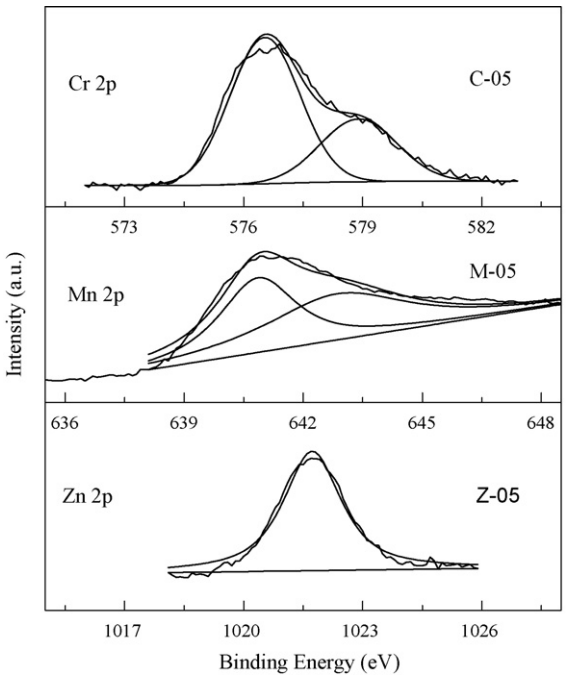

Fig. 1. XPS patterns of the as-prepared catalysts.

At the same time, compared with the narrow peak of Zn $2p_{1/2}$ in the Zn-promoted catalyst, the Mn $2p_{3/2}$ and Cr $2p_{3/2}$ peaks are widened, which imply multi-valence ions presented in the catalysts. Specifically, Mn $2p_{3/2}$ can be fitted by two peaks with the binding energy of 641.1 eV and 642.3 eV, indicating the coexistence of Mn^{3+} and Mn^{4+} in FeMn catalyst [25]. Similarly, the Cr $2p_{3/2}$ peak can be divided into two peaks at the binding energy of 576.5 eV and 578.9 eV, which means the coexistence of Cr^{3+} and Cr^{6+} in FeCr catalyst [26–29].

3.3. Crystallite structure of the catalyst

The crystallite structure of the as-prepared catalysts was characterized by XRD, MES and EXAFS. The results of XRD (see Supplementary information, Fig. S2) show that all diffraction peaks of the FeMn and FeCr catalysts are similar to that of the typical α-Fe_2O_3 (JCPDS 84-0306). While the FeZn catalyst presents two additional small diffraction peaks at 29.9° and 56.8° except for the typical diffraction peaks of α-Fe_2O_3 phase. According to the JCPDS data, the diffraction peaks at 29.9° and 56.8° of the FeZn catalyst can be attributed to (2 2 0) and (3 3 3) planes of $ZnFe_2O_4$ phase (JCPDS 82-1049) with cubic franklinite spinel-type structure [19]. Since the strongest peak (3 1 1) of $ZnFe_2O_4$ is closed to that of (1 1 0) of α-Fe_2O_3, it is difficult to discriminate it. To find the effect of promoters on the crystallite structure of α-Fe_2O_3, the lattice parameters of the promoted catalyst were also calculated from XRD. The results show that the lattice parameters are a = 5.025 Å and c = 13.71 Å for C-05 and a = 5.025 Å and c = 13.72 Å for M-05, respectively, which are smaller than that of the pure α-Fe_2O_3 lattice (a = 5.034 Å, c = 13.75 Å). However, the Zn-promoted catalyst

Table 2
Comparison of the composition between surface and bulk of the catalysts.

Catalysts	M/Fe (×10^2 atomic ratio)		Surface/bulk
	Surface (from XPS)	Bulk (from ICP)	
Z-05	12.8	5.5	2.3
M-05	18.3	4.8	3.8
C-05	10.6	5.1	2.1

Table 3
Mössbauer parameters of the as-prepared catalysts.

Catalysts	Phases	Mössbauer parameters			Area (%)
		IS (mm/s)	QS (mm/s)	Hhf (kOe)	
Fe_2O_3	α-Fe_2O_3	0.35	−0.18	513	100
Z-05	α-Fe_2O_3	0.39	−0.18	513	88.6
	$ZnFe_2O_4$	0.36	0.36	–	11.4
M-05	α-$(Fe_{1-x}Mn_x)_2O_3$	0.37	−0.19	510	100
C-05	α-$(Fe_{1-x}Cr_x)_2O_3$	0.38	−0.17	504	100

Z-05 has the similar lattice parameters (a = 5.033 Å and c = 13.75 Å) to that of α-Fe_2O_3.

MES parameters of the fresh catalysts were summarized in Table 3. As listed in Table 3, the MES spectra of Cr- and Mn-promoted catalysts is composed of one single sextet, and Zn-promoted catalyst shows one sextet and one doublet (see Supplementary information, Fig. S3). The isomer shift (IS), quadrupole splitting (QS) and hyperfine field (Hhf) of the sextet for unpromoted α-Fe_2O_3 are 0.35 mm s^{-1}, −0.18 mm s^{-1} and 513 kOe, respectively [5,11]. The IS and QS of the promoted catalysts are similar to that of α-Fe_2O_3. However, the Hhf values of the Zn-, Cr- and Mn-promoted catalysts decrease to 513 kOe, 510 kOe

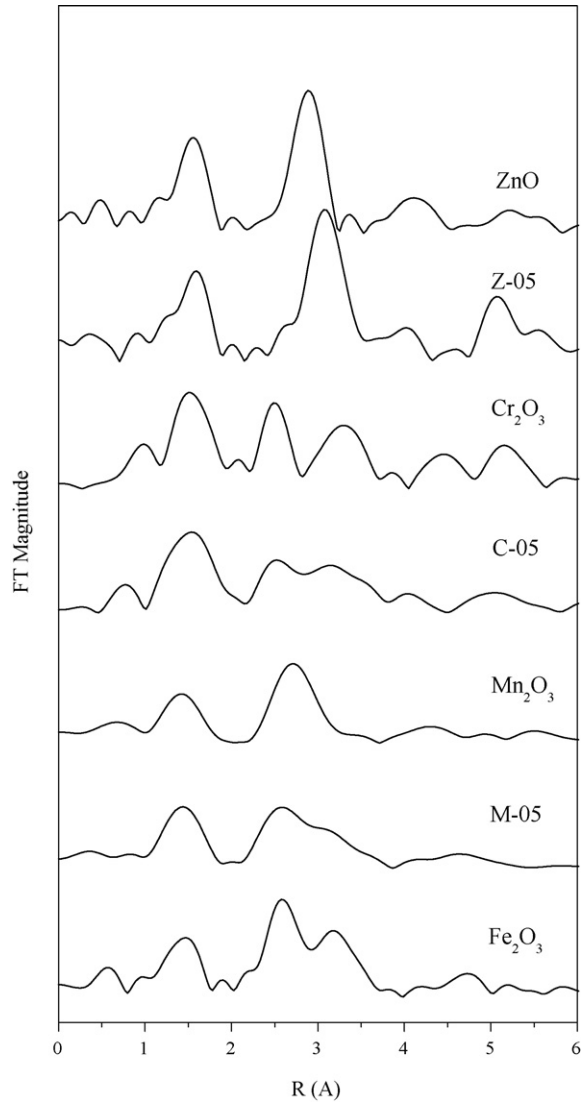

Fig. 2. k^3-weighted Fourier transform magnitudes of EXAFS spectra of the as-prepared catalyst and reference compounds.

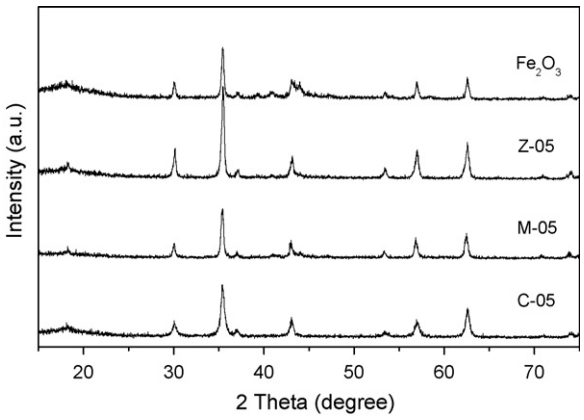

Fig. 3. XRD patterns of the reduced catalysts.

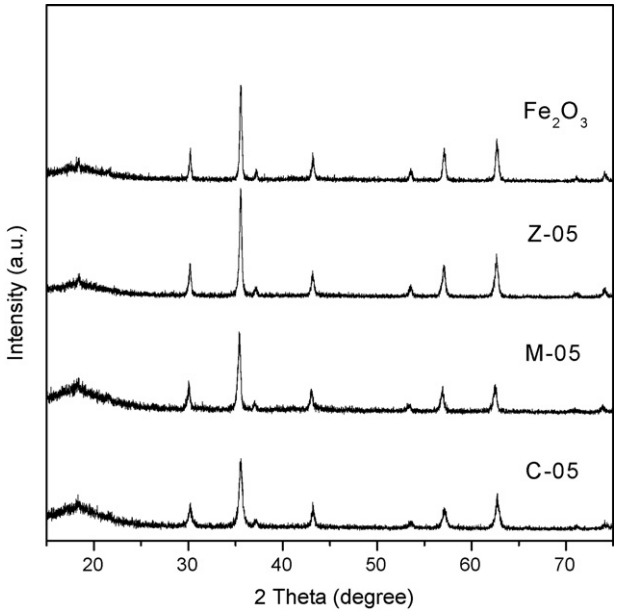

Fig. 5. XRD patterns of the used catalysts.

and 504 kOe, respectively. It is noteworthy that the IS and QS values of the doublet in Zn-promoted catalyst are 0.36 mm s^{-1} and 0.36 mm s^{-1}, respectively. Both of them are well consistent with that of the typical $ZnFe_2O_4$ [30–32].

Furthermore, the EXAFS experiments were also done and the k^3-weighted Fourier transform of the EXAFS spectra of the promoted catalysts and the reference compounds are shown in Fig. 2. From Fig. 2, it can be seen that there are three peaks at 1.49 Å, 2.55 Å and 3.20 Å observed for α-Fe_2O_3 [33]. In the Fourier transform of the Mn K-edge, there are two peaks at 1.45 Å and 2.71 Å observed for Mn_2O_3 [34], while three peaks at 1.49 Å, 2.55 Å and 3.20 Å for Mn-promoted catalyst, which is very similar to those for α-Fe_2O_3. At the same time, it is found that the peaks at 2.55 Å and 3.20 Å are significantly diminished in the promoted catalyst M-05. In the Fourier transform of the Cr K-edge, there are three peaks at roughly 1.49 Å, 2.55 Å and 3.20 Å for both Cr-promoted catalyst and the reference compound Cr_2O_3 [35], which are very similar to those for Fe_2O_3. Similar to Mn-promoted catalyst, the Cr-promoted catalyst C-05 also obviously shows two reduced peaks at 2.55 Å and 3.20 Å. The features of Zn-promoted catalyst are different from those of the reference compound ZnO obviously in the Fourier transform of the Zn K-edge. There are two peaks at 1.55 Å and 2.90 Å observed for ZnO, while two peaks at about 1.55 Å and 3.10 Å observed for Zn-promoted catalyst. $ZnFe_2O_4$ compounds with two peaks at 1.55 Å and 3.10 Å in Zn K-edge was reported by Lee and Anderson [36], thus it can be concluded that $ZnFe_2O_4$ compound appears in the catalyst Z-05.

The XRD patterns of the reduced catalysts are shown in Fig. 3. It can be seen that they are mainly composed of magnetite (Fe_3O_4), except that the unpromoted catalyst has some iron carbide phase with broad and weak peaks at 2θ of 39.3°, 40.9°, 43.9°, 44.9° and 47.2°. Due to the poor crystallographic nature and the relatively low content of iron carbide in the promoted catalysts after reduction, there is no iron carbide detected in the XRD profiles.

The MES results of the reduced catalysts are shown in Fig. 4 and Table 4. It can be clearly seen that the unpromoted catalyst is mainly composed of magnetite (Fe_3O_4) and iron carbide

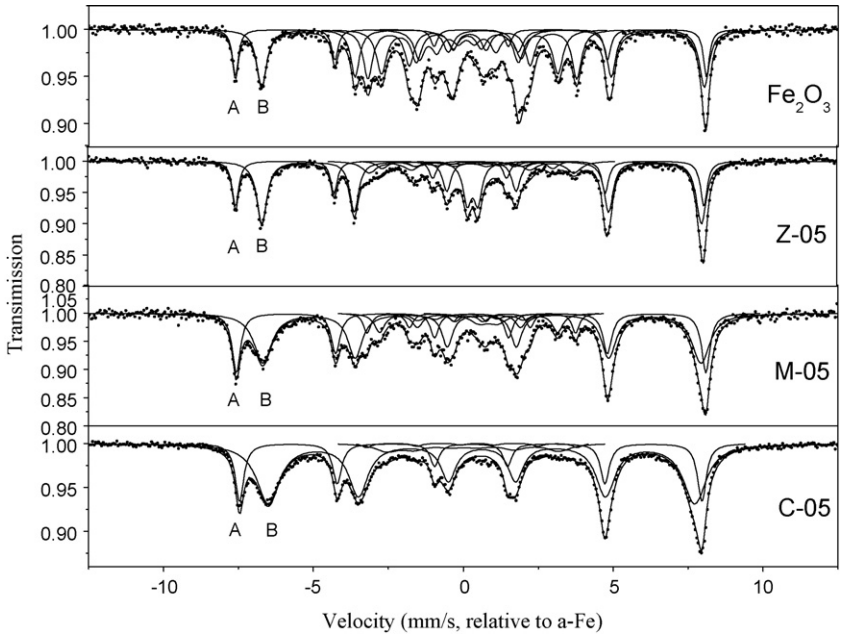

Fig. 4. Mössbauer patterns of the reduced catalysts.

Table 4
Mössbauer parameters of the reduced catalysts.

Catalysts	Phases		Mössbauer parameters			Area (%)
			IS (mm/s)	QS (mm/s)	Hhf (kOe)	
Fe_2O_3	Fe_3O_4	A	0.25	−0.01	489	13.8
		B	0.65	−0.01	459	27.8
	χ-Fe_5C_2	I	0.25	0.09	217	22.5
		II	0.17	0.07	183	21.6
		III	0.16	0.13	106	14.3
Z-05	Fe_3O_4	A	0.25	0.00	486	25.4
		B	0.64	0.01	456	41.5
	χ-Fe_5C_2	I	0.29	0.04	212	7.2
		II	0.13	0.08	177	2.6
		III	0.20	0.01	110	7.7
	$ZnFe_2O_4$		0.34	0.36		7.1
	Fe^{2+} (spm)		1.13	0.46		8.5
M-05	Fe_3O_4[a]	A	0.27	−0.02	487	26.2
		B	0.62	0.00	455	47.0
	χ-Fe_5C_2	I	0.24	0.05	216	7.8
		II	0.18	−0.01	185	10.4
		III	0.17	0.14	110	4.4
	Fe^{2+} (spm)		0.83	0.62		4.2
C-05	Fe_3O_4[a]	A	0.25	−0.02	479	31.5
		B	0.60	−0.05	443	58.4
	χ-Fe_5C_2	I	0.38	−0.19	218	1.8
		II	0.17	0.30	179	8.3

[a] Fe_3O_4 is present in the form of solid solution.

(χ-Fe_5C_2) after reduction, with a high iron carbide content of 58.4%. In contrast, the addition of promoters has a significant impact on the content of iron carbide. The iron carbide content in the Zn-, Mn- and Cr-promoted catalysts is 17.5%, 22.6% and 10.1%, respectively. It is noteworthy that superparamagnetic (spm) Fe^{2+} is observed with contents of 8.5% and 4.2% for Zn- and Mn-promoted catalysts, respectively, which can be assigned to the wustite (FeO) phase stabilized by the substitution of the promoter ions [10,21,37,38].

The crystallite structure of the used catalysts was also characterized by XRD and MES. Fig. 5 shows the XRD patterns of the catalysts after reaction. As shown in Fig. 5, all used catalysts only show similar diffraction peaks for Fe_3O_4 phase. The diffraction peaks of iron carbide phase disappeared in the unpromoted catalyst after reaction.

The MES results of used catalysts are shown in Fig. 6 and Table 5. From Table 5, it can be seen that the content of spinel phase (Fe_3O_4) is 90.7%, 82.8% and 85.1% in α-Fe_2O_3, Z-05 and M-05, and the content of iron carbide phase is only 9.3%, 11.7% and 14.1%, respectively. The magnetite phase is the only phase detected in C-05 catalyst. The amount of iron carbide in catalysts decreased significantly during reaction process. Correspondingly, the magnetite content increased obviously. The phenomenon may be due to the oxidation of iron carbide by H_2O and CO_2 during reaction [2,39–41]. Moreover, the significant decrease of Fe^{2+} (spm) content observed in Zn and Mn-promoted catalysts may be also due to the oxidization.

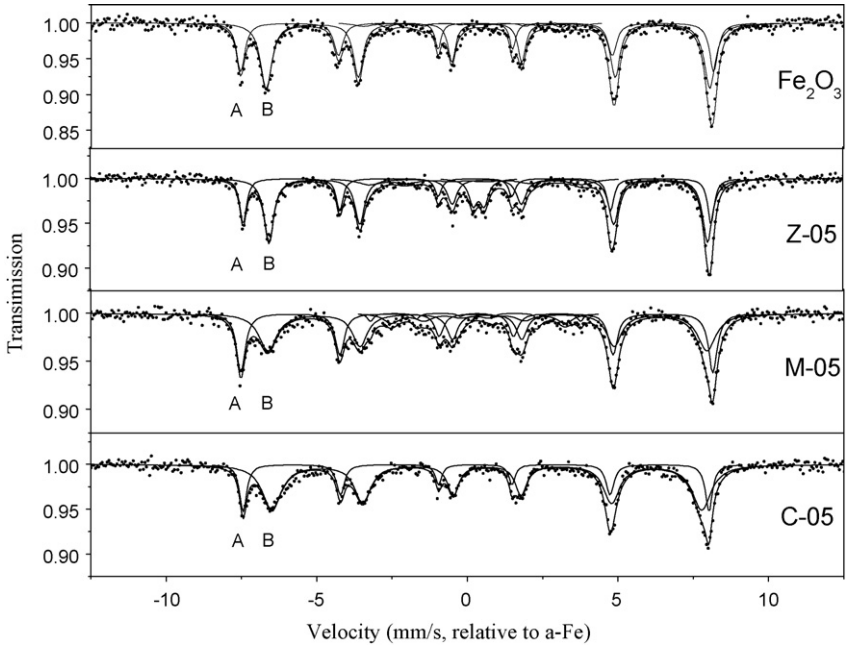

Fig. 6. Mössbauer patterns of the used catalysts.

Table 5
Mössbauer parameters of the used catalysts.

Catalysts	Phases		MÖssbauer parameters			Area (%)
			IS (mm/s)	QS (mm/s)	Hhf (kOe)	
Fe_2O_3	Fe_3O_4	A	0.29	0.06	488	32.3
		B	0.66	0.04	458	58.4
	χ-Fe_5C_2	I	0.22	−0.29	220	5.3
		II	0.22	−0.01	180	4.0
Z-05	Fe_3O_4[a]	A	0.32	0.07	483	29.4
		B	0.70	0.05	453	53.4
	χ-Fe_5C_2		0.19	0.24	220	11.7
	$ZnFe_2O_4$		0.41	0.37		5.3
	Fe^{2+} (spm)		1.12	0.60		0.2
M-05	Fe_3O_4[a]	A	0.31	0.02	487	37.0
		B	0.66	0.01	453	48.1
	χ-Fe_5C_2	I	0.20	−0.02	207	9.4
		II	0.30	0.12	173	4.7
	Fe^{2+} (spm)		0.69	0.58		0.8
C-05	Fe_3O_4[a]	A	0.28	0.03	481	27.9
		B	0.65	−0.01	444	72.1

[a] Fe_3O_4 is present in the form of solid solution.

3.4. Reduction and carburization behaviors

The effects of promoters on the reduction behavior were measured by H_2-DTG and CO-TPR. The H_2-DTG profiles are shown in Fig. 7.

As shown in Fig. 7, the profiles of all catalysts contain two obvious reduction peaks, corresponding to the reduction of α-Fe_2O_3 to Fe_3O_4 and Fe_3O_4 to α-Fe, respectively. It can be seen that the first reduction peak of α-Fe_2O_3 appears at about 331 °C. The first reduction peak of Z-05 is similar to that of α-Fe_2O_3, while that of the catalysts M-05 and C-05 obviously shifts to 346 °C and 357 °C, respectively. Except for the C-05 catalyst, the second reduction peaks of the other catalysts are almost at the same temperature (542 °C or so). The second reduction peak of C-05 moves to high temperature and shows a broad band. In addition, a small peak of the sublimation of ZnO is also observed at about 690 °C in Zn-promoted catalyst [42].

CO-TPR was also used to study the catalysts reduction and carburization behaviors and the results are shown in Fig. 8. As shown in Fig. 8, the three-stage CO consumption peaks observed for the unpromoted α-Fe_2O_3 is characteristic of the reduction of α-Fe_2O_3 to Fe_3O_4, Fe_3O_4 carburization to Fe_xC_y and probably a carbon peak from Boudouard reaction. Similar reduction behaviors were obtained for Z-05, except that the peak of carbon deposition moves slightly to high temperature. Similar two-stage process for M-05 and C-05 is observed with no carbon deposition peak identified. The first reduction peak appears at the same temperature of 278 °C in both α-Fe_2O_3 and Z-05 catalysts, while that of M-05 and C-05 shifts to 308 °C and 318 °C, respectively. The second peak temperature of M-05 (450 °C) is lower than that of α-Fe_2O_3 and Z-05 (470 °C), while that of C-05 is the highest (560 °C).

3.5. CO_2-TPD results

CO_2-TPD was used to investigate the effect of promoters on the surface basicity of the catalysts and the curves are presented in Fig. 9. It is shown that only one desorption peak is seen at about 77 °C for unpromoted α-Fe_2O_3, which can be attributed to the desorption of the weakly chemisorbed CO_2 [43]. Besides the low temperature desorption peak, the promoted catalysts show an additional peak at higher temperatures of 265 °C, 320 °C and 340 °C for Mn, Cr and Zn promoters, respectively, in which the peak intensity of Cr- and Mn-promoted catalysts is more obvious than that of Zn-promoted catalyst. These results show that there

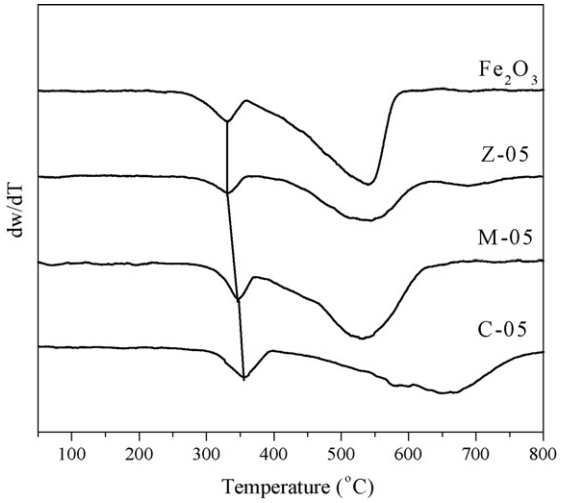

Fig. 7. H_2-DTG patterns of the as-prepared catalysts.

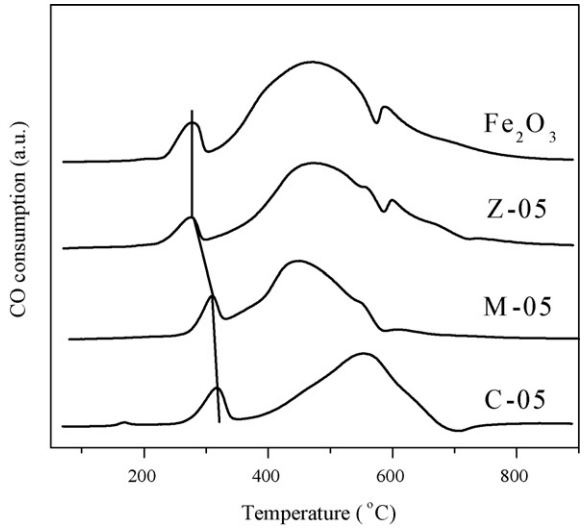

Fig. 8. CO-TPR patterns of the as-prepared catalysts.

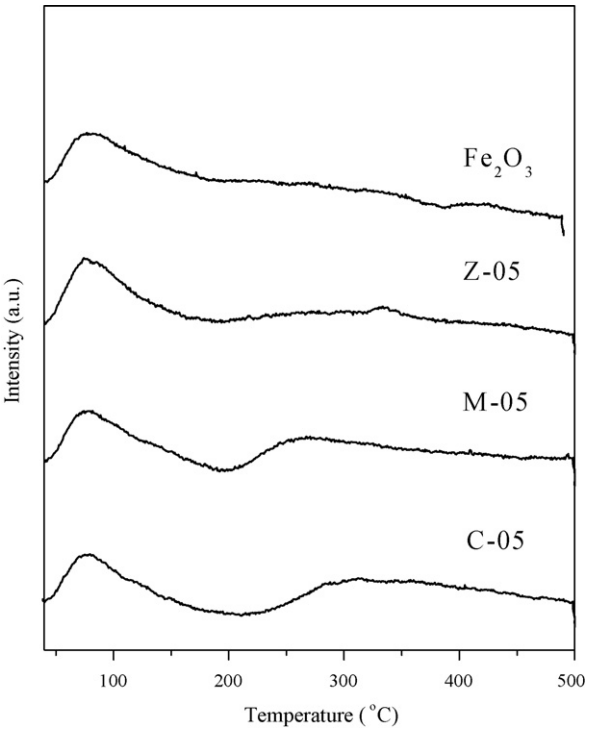

Fig. 9. CO_2-TPD patterns of the as-prepared catalysts.

are strong basic sites in these promoted catalysts, where the Cr- and Mn-promoted catalysts have more surface basic sites.

3.6. Activity and selectivity

3.6.1. Catalyst activities

The effects of the promoters on the FTS activity of the catalysts are shown in Fig. 10. For the unpromoted α-Fe_2O_3, the catalytic activity is at a high level (92%) at the beginning of the reaction, but quickly decreases with time on stream (TOS) to 32% after 160 h reaction, and then reaches a steady state till the end of reaction. The deactivation is also observed for the Z-05 catalyst. The catalytic activity is as high as 95%, and then gradually decreases to 52% at the end of the reaction. In contrast, the Mn-promoted catalyst M-05 achieves the steady state of about 45% CO conversion after 50 h induction time. The catalytic performance of the catalyst C-05 in terms of stability is similar to that of the Mn-promoted catalyst. With 50 h induction time, its catalytic activity is stabilized at about 23%. However, the catalytic activity of C-05 is much lower than that of the catalyst M-05.

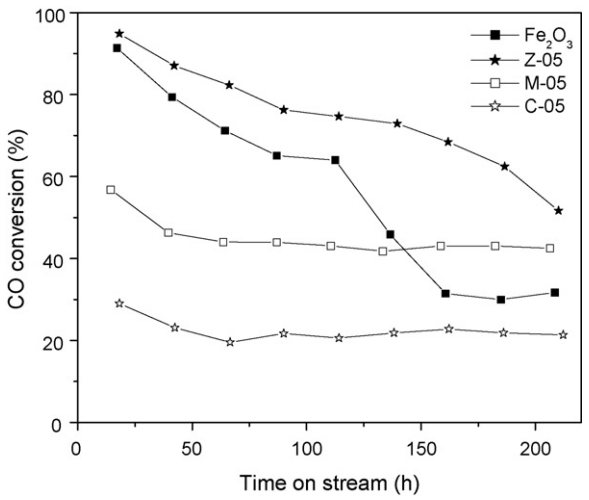

Fig. 10. CO conversion of the catalysts.

3.6.2. Product selectivity

The hydrocarbon product distribution of the catalysts is listed in Table 6. It can be seen that the selectivity to methane of the catalyst M-05 (12–13 wt%) is lower than that of C-05 (23–24 wt%) obviously, while that of the unpromoted α-Fe_2O_3 and Zn-promoted Z-05 is slightly higher, which is in the range of 27–33 wt%. The variation of the selectivities of C_{5+} and $C_{2-4}^{=}$ (in C_{2-4} hydrocarbon) shows the opposite trend with that of methane selectivity in the catalysts. The selectivity to C_{5+} for promoted catalysts Z-05, C-05 and M-05 is 20–23 wt%, 31–34 wt%, and 44–47 wt%, respectively, and that for unpromoted α-Fe_2O_3 is 23–28 wt%. The olefin selectivity of $C_{2-4}^{=}$ for Z-05 is close to the value of unpromoted α-Fe_2O_3 (around 0.26–0.32), while that of C-05 and M-05 is in the range of 0.43–0.44 and 0.75–0.76, respectively. At the same time, it can be seen that the catalyst Z-05 shows the highest selectivity to CO_2 (33–37 mol%) in promoted catalysts, while the selectivity to CO_2 is only 19–22 mol% for C-05 and M-05 which is slightly lower than that of unpromoted α-Fe_2O_3 (24–27 mol%). In summary, the catalysts C-05 and M-05 show low methane selectivity, high C_{5+} hydrocarbon selectivity and high olefin selectivity, where the variation of these selectivities in M-05 is more obvious than that in C-05.

4. Discussion

4.1. Textural properties of the fresh catalysts

From Table 1, it can be clearly seen that the Mn and Cr promoters can enhance the dispersion of iron phase, while this is not the case for Zn-promoted catalyst. This result is also validated by the measured crystallite size of the catalysts (Table 1).

The difference in surface area can be explained by the crystallite structure of the catalysts. In Section 4.3, the analysis of phases of the fresh catalysts reveals that Mn^{3+} and Cr^{3+} are incorporated into the lattice of α-Fe_2O_3 and locate at the substitutional site of Fe^{3+} in Mn- and Cr-promoted catalysts, while $ZnFe_2O_4$ compound is formed in Zn-promoted catalyst which leads to the aggregation of Zn^{2+} ions. Thus, the higher BET surface area for Mn- and Cr-promoted catalysts are obtained due to their better dispersion than that of Zn promoter.

Recent studies showed that coordinately unsaturated sites (CUS) are present at the surface of the ferrihydrite crystals and coprecipitation of Fe^{3+} with other cations such as M = Si^{4+}, Al^{3+} and Mo^{6+} can enlarge the surface area of hematite derived from ferrihydrite. This can be explained by the presence of these cations adsorbed on the surface of ferrihydrite crystallites which inhibit the growth of ferrihydrite crystallites during calcination to yield hematite [34,44,45]. Similar result was observed in FeCe system [46]. It is well known that silica gel and alumina gel contain lots of hydroxyls. When they are coprecipitated with Fe^{3+} in solution, their ions could be adsorbed on the CUS in the form of micelles which can prevent the conglomeration of hematite in the subsequent calcination step.

4.2. Surface composition of fresh catalysts

The results of XPS show the enrichment of promoter atoms on the surface of catalysts, in which Mn-promoted catalyst shows the higher enrichment of promoters on the surface of the catalyst. Previous studies also reported the enrichment of Mn promoter on the surface of catalysts, which was believed to be one of the reasons for the improved olefin selectivity over Mn-promoted iron catalyst

Table 6
Activity and selectivity of the catalysts.[a,b].

Catalysts	α-Fe_2O_3		Z-05		M-05		C-05	
TOS (h)	137	209	140	210	133	206	138	212
CO conversion (%)	45.9	31.8	72.9	51.7	41.8	42.5	21.9	21.4
(CO + H_2) conversion (%)	37.6	29.4	52.6	39.6	36.4	36.9	17.0	17.5
CO_2 selectivity (mol%)	27.2	24.1	36.5	33.2	21.5	20.4	19.7	18.9
H_2/CO (in tail gas)	2.4	2.1	4.5	2.9	2.3	2.3	2.2	2.1
H_2/CO usage	1.4	1.8	1.3	1.4	1.6	1.6	1.3	1.4
Hydrocarbon selectivities (wt.%)								
CH_4	26.6	32.9	29.2	27.1	12.6	12.3	22.7	24.2
C_{2-4}	45.8	43.9	50.3	49.9	43.1	41.1	43.6	45.2
C_{5+}	27.6	23.2	20.5	23.0	44.3	46.6	33.7	30.6
Olefin selectivity in C_{2-4}								
$C_{2-4}^{=}$	0.32	0.31	0.26	0.31	0.76	0.75	0.44	0.43

[a] Reduction conditions: 0.1 MPa, H_2/CO = 2.0, S.V. = 1000 ml/(g h), 280 °C.
[b] Reaction conditions: 1.5 MPa, H_2/CO = 2.0, S.V. = 2000 ml/(g h), 260 °C.

[5,47,48]. However, the mechanism of the Mn promoter enrichment is still unclear. The analysis of the Mn 2p core level reveals Mn^{4+} species existence on the surface, showing that part of Mn atoms have been oxidized to higher valence in catalyst [25,49–52]. Therefore, it is possible that the oxidation of Mn promoter leads to the surface enrichment of Mn. On the other hand, the enrichment of promoters in Cr-promoted catalyst is lower than that in Mn-promoted catalyst following the oxidation treatment, which suggests further study is imperative for the Mn, Zn and Cr promoters during the enrichment process.

4.3. Crystallite structure change of catalysts

In XRD results, the phases of Cr and Mn promoters were not observed in Cr- and Mn-promoted catalysts. Many studies reported that FeCr and FeMn solid solutions were formed during coprecipitation [10,51,53,54]. Thus, it is possible that the disappearance of diffraction peaks for the phases of Cr and Mn promoters is due to the dissolving of Cr or Mn atoms in the hematite phase. This can be proved by the change of the lattice parameters. The calculated lattice parameters for the phase of hematite in C-05 and M-05 is slightly lower than that of the pure α-Fe_2O_3 lattice (see Section 3.3), which indicates that Mn and Cr atoms are doped into the lattice of α-Fe_2O_3. The radii of Fe^{3+}, Mn^{3+}, Cr^{3+} and Zn^{2+} is 0.64 Å, 0.66 Å, 0.63 Å and 0.76 Å, respectively. The radii of Mn^{3+} and Cr^{3+} is very close to that of Fe^{3+}, while the radii of Zn^{2+} is larger than that of Fe^{3+} obviously. Combining with the crystallite structure of the promoted catalysts, it can be seen that the similarity in ionic radius of metal promoters and iron probably facilitates the solid solution formation, while a large difference in their radii may lead to the formation of a compound.

Some researchers [10,55,56] found that the substitution of Mn atoms in the phase of wustite (FeO) could enlarge the cell parameters of the ferric phase, where the ionic radius of Mn^{2+} (0.80 Å) is larger than that of Fe^{2+} (0.74 Å). Accordingly, it is expected that the lattice dimensions of the FeMn solid solution should be enlarged. On the contrary, a cell shrinkage of the catalyst M-05 is observed in our XRD results. Similar results were also reported by Maiti et al. [10]. Previous studies show that α-Fe_2O_3 belongs to corundum structure, while Mn_2O_3 exhibits a typical bixbyite structure similar to that of CaF_2 with some vacant oxygen sites [11,57–59]. Therefore, the cell shrinkage probably comes from the reconstruction for Mn substituted sample.

The structural change of promoted catalysts also could be observed by MES results. It is generally accepted that the addition of Cr or Mn could decrease the Hhf value of iron phases in catalysts due to the magnetic dilution effect by the form of FeCr or FeMn solid solution [60–62]. Compared with the Hhf value of α-Fe_2O_3, that of Mn-, and Cr-promoted catalysts also decreased to some extent, which confirms the existence of the FeMn and FeCr solid solutions in them. In present study, the lowest Hhf value for Cr-promoted catalyst is observed, which is in agreement with previous work by Lee et al. [62]. Zn-promoted catalyst shows the same Hhf value to that of α-Fe_2O_3 phase, indicating the phase separations between Zn and Fe phases in catalyst.

Besides of XRD and MES, the structural change of promoted catalysts was also followed by EXAFS results. It can be found from Fig. 2 that the features of the Fourier transform curve of M-05 are virtually identical to those of α-Fe_2O_3 rather than Mn_2O_3 in Mn K-edge, indicating that the local environment of the Mn atoms is similar to that of the Fe atoms and Mn atoms are incorporated into the lattice of α-Fe_2O_3 and locate at the substitutional site of Fe atoms. Meanwhile, the peaks at 2.55 Å and 3.20 Å are significantly diminished in the promoted catalyst M-05, implying that most of Mn atoms lost its long-range-ordered properties to form an amorphous phase in catalyst for the substitution of Mn. Thus, it can be concluded that the FeMn solid solution formed in the catalyst M-05. The features of C-05 in Cr K-edge are very similar to those of the reference compounds α-Fe_2O_3 and Cr_2O_3. However, in contrast to the second and third peaks of the reference compounds, their intensity in Cr-promoted catalyst decreases obviously, indicating that most of Cr atoms lost its long-range-ordered properties to form an amorphous phase in catalyst for the substitution of Cr. For the catalyst Z-05, two peaks at 1.55 Å and 3.10 Å reliably show the presence of $ZnFe_2O_4$ compounds in Zn K-edge. These results are all consistent with the analysis of XRD and MES.

Although the FeMn and FeCr solid solution and $ZnFe_2O_4$ compound were detected in the fresh catalysts, it is difficult to distinguish them from the iron phases by XRD due to the complexity and poor crystallite structure of the reduced catalysts. But, the phase of promoters can be clearly discriminated by MES.

From Fig. 4, it can be found that the sextet corresponding to B- Fe_3O_4 in Cr- and Mn-promoted catalyst is broadened obviously, which may be due to the incorporation of Mn and Cr atoms into the lattice of magnetite (Fe_3O_4) [62]. Moreover, the Hhf value of the catalyst C-05 is smaller than that of other promoters apparently, which suggests a stronger magnetic dilution of the Cr promoter than that of the Mn promoter. In the Zn-promoted catalyst, the spectral contribution of the doublet of $ZnFe_2O_4$ is 7.1% in the reduced catalyst, which is slightly lower than that in the fresh catalyst (11.4%), indicating a fraction of $ZnFe_2O_4$ compound is reduced. According to literature [63], the structure of compound $ZnFe_2O_4$ was modified according to the following reaction during reduction: $ZnFe_2O_4 + H_2 \rightarrow ZnFe_2O_{4-\delta} + \delta H_2O$. Hence, it suggests that the partially reduced $ZnFe_2O_4$ compound were transformed into the $Zn_xFe_{1-x}O$ phase in Z-05, which is probably undetectable with XRD.

This agrees well with our previous study [64] on the reduction of FeZn catalysts where the ZnO-doped FeO wustite phase was confirmed. Consequently, Zn-promoted catalyst may mainly exist as the $ZnFe_2O_4$ compound with only negligible amount converted to $Zn_xFe_{1-x}O$.

Regarding the effect of promoters on iron catalyst during reduction, it can be concluded that the formation of hardly reducible $ZnFe_2O_4$ suppresses the catalyst reduction and hence the extent of carburization for the Zn-promoted catalyst. For Mn- and Cr-promoted catalysts, the formation of FeMn and FeCr solid solutions strongly inhibits the reduction of catalysts which leads to the low degree of carburization.

For the used catalysts, it can be apparently found that the sextet corresponding to B-Fe_3O_4 in Cr- and Mn-promoted catalyst is also broadened (see Fig. 6) and the Hhf value of Cr-promoted catalyst decreases more obviously than that of Mn-promoted catalyst (see Table 4), indicating the existence of FeMn and FeCr solid solutions in catalysts [62], which is similar to the observation in the reduced catalysts. In Zn-promoted catalyst Z-05, the compound $ZnFe_2O_4$ is still observed with trace of Fe^{2+} (spm). Therefore, it can be seen that Zn promoter is the form of the compound $ZnFe_2O_4$ in the used catalysts besides trace of $Zn_xFe_{1-x}O$ phase. In contrast, the Mn and Cr promoters exist as solid solutions of FeMn and FeCr in the phase of Fe_3O_4, respectively.

4.4. Reduction and carburization behaviors

Given the fact of FeMn and FeCr solid solutions in Mn- and Cr-promoted catalysts from the analysis of crystallite structure of the catalysts, it can be seen that these mixed-oxide phases obviously inhibit the catalyst reduction from α-Fe_2O_3 to Fe_3O_4, in which the inhibition of Cr promoter is more intense than that of Mn promoter from the results of H_2-DTG and CO-TPR. At the same time, it also can be seen that the incorporation of Cr restrains the further reduction of Fe_3O_4 intensely, while incorporation of Mn promoter almost has no effect on the Fe_3O_4 further reduction, showing that the effect of Mn promoter is different from that of Cr promoter. This can be ascribed to the appearance of the major intermediate MnO-doped FeO wustite phase during the reduction, as has been seen in Section 3.3 for the reduced catalysts. Because the separation of phases between α-Fe_2O_3 and $ZnFe_2O_4$ occurred in Zn-promoted catalyst, there is no shift of the first reduction peak observed in the process of reduction, and the peak only represents the reduction of α-Fe_2O_3 to Fe_3O_4. The second reduction peak can be ascribed to the further reduction of Fe_3O_4 and $ZnFe_2O_4$ in Zn-promoted catalyst [63]. It is worth noting that the third peak disappears for C-05 and M-05 in CO-TPR profiles, implying Cr and Mn promoters could inhibit the deposition of carbon in catalysts. This probably is correlated with the characteristics of FeCr and FeMn solid solutions.

4.5. Activity and selectivity

It is generally accepted that iron carbide phase is the active phase in FTS [65–67]. Therefore, the variation of the catalytic activity of promoted catalysts can be explained by the change of the iron carbid phase in the bulk of the reduced or used catalysts. Ding et al. [68] reported that the catalytic activity increased with the degree of carburization of the catalyst in the near-surface regions during FTS. Similar result was also reported by Li et al. [69] in which they showed that only a fraction of iron carbides on the surface layers promoted the catalytic activity in FTS reaction, regardless of the chemical nature of the residual bulk Fe_3O_4 or iron carbides. In addition, it is also reported that iron carbide nodules are generally present in working iron catalyst as an eggshell layer surrounding large Fe_3O_4 particles [70]. Thus, it can be inferred that the initial high catalytic activity in unpromoted catalyst (α-Fe_2O_3) is probably due to the large amount of iron carbides (58.4%) which presented both on the surface and in the bulk of the catalyst. Compared with unpromoted α-Fe_2O_3, Mn-promoted catalyst shows the low content of iron carbide (22.6%), suggesting a lower carburization degree in the catalyst which possibly occurred mainly on the surface of the catalyst. This explains the lower catalytic activity than that of unpromoted catalyst. Similar promotional effect was also obtained for Cr-promoted catalyst C-05. The lowest degree of carburization (11.1%) determines its lowest catalytic activity. However, unlike the FeCr and FeMn catalysts, FeZn catalyst shows similar catalytic activity to that of α-Fe_2O_3 at a relatively lower degree of carburization. It has been reported that ZnO is a good hydrogenation catalyst and hydrogen spillover has been observed with ZnO acting as a reservoir of hydrogen during methanol synthesis [71–73]. Consequently, the higher catalytic activity of Z-05 could be partially attributed to the effect of ZnO. Additionally, the high catalytic activity of Z-05 is associated with its high selectivity to CO_2 (i.e. high WGS activity).

Table 7
Ratio of FeC_x/FeO_x in the reduced and used catalysts.

Catalysts	FeC_x/FeO_x	
	Reduced catalysts[a]	Used catalysts[a]
Fe_2O_3	1.4	0.1
Z-05	0.2	0.1
M-05	0.3	0.2
C-05	0.1	0

[a] Calculated from the ratio of Fe_5C_2/Fe_3O_4 or $Fe_5C_2/(Fe_3O_4+ZnFe_2O_4)$ for Z-05 in Tables 4 and 5, respectively.

To explain the deactivation observed in the catalysts, Table 7 shows the ratio change of FeC_x/FeO_x in catalysts during reaction. It can be found that the ratio of FeC_x/FeO_x in unpromoted catalyst decreases from 1.4 to 0.1 after reaction. Simultaneously, the catalytic activity decreases from 92% to 32%. These results indicate that the oxidation of iron carbide leads to the deactivation of the unpromoted catalyst. The ratio of FeC_x/FeO_x for C-05, M-05 and Z-05 decreases from 0.2, 0.3 and 0.1 to 0.1, 0.2 and 0, respectively. Compared with the oxidation in unpromoted catalyst, the oxidization of iron carbide in promoted catalyst is not serious, which is consistent with their lower deactivation rate (as shown in Fig. 10). These results show that the addition of promoters could stabilize the iron carbide phases obviously, and further improve the stability of the catalysts. Combining with the crystallite structure of the catalysts, it is found that the formation of solid solution is more favorable than that of compound to improve the stability of the catalysts.

From Table 6, it can be found that the Cr- and Mn-promoted catalysts show lower methane selectivity, higher olefin and C_{5+} hydrocarbon selectivity, where the variation of these selectivities in Mn-promoted catalyst is more obvious than those in Cr-promoted catalyst. The difference in the selectivity of these catalysts can probably be explained from the results of catalyst characterization. It is well known that surface basic sites existing on catalyst facilitate the CO dissociative adsorption while inhibit the H_2 dissociative adsorption, thus leading to lower methane formation, higher olefin and heavy hydrocarbon selectivity [3,6]. From CO_2-TPD results, Cr- and Mn-promoted catalysts also have more strong surface basic sites. Therefore, these selectivities are correlated with their surface basic sites. For Mn-promoted catalyst, the more obvious variation of these selectivities can attribute to the enrichment of Mn atoms on the surface of catalyst which can also result in the lower methane formation, higher light olefin and heavy hydrocarbon selectivity [5,47,48]. Furthermore, it should be noted that the differences of these catalysts in carburization and sintering extent during reduction and reaction process may also affect the product selectivity. It is noteworthy that the FeZn catalyst (Z-05) shows the high-

est initial catalytic activity among both the unpromoted α-Fe_2O_3 and promoted catalysts, but deactivates even with the presence of $ZnFe_2O_4$ compound which is believed to be able to stabilize the surface active sites for FTS. The stability and hydrocarbon selectivity maybe improved by the incorporation of structural and chemical promoters. Further study on the detailed mechanism of the catalyst structure transformation under reaction condition is imperative.

5. Conclusions

Effects of transition metals Zn, Mn and Cr promoters on the catalytic properties of Fe-based catalysts can be classified into two kinds: the compound interaction and the solid solution interaction. For the Zn-promoted catalyst, Zn promoter forms the $ZnFe_2O_4$ compound, which results in the phase separations between Zn and Fe phases. While for the FeMn and FeCr bimetallic catalysts, the solid solution interaction of these mixed-oxide systems take place, where Mn and Cr atoms probably enter the lattice of hematite with evidence from XRD, MES and EXAFS results.

Due to the higher dispersion, the FeMn and FeCr catalysts show higher BET surface area than that of FeZn catalyst. The enrichment of promoters on the surface of the catalysts is noticeable for all catalysts, especially for Mn-promoted catalyst which shows the highest enrichment level upon exposure to oxidation environment. During the catalyst reduction step, the solid solutions formed in the FeMn and FeCr catalysts inhibit the reduction of α-Fe_2O_3 to Fe_3O_4, while this effect is not so significant in the FeZn catalyst with the $ZnFe_2O_4$ compound.

The catalytic performance in the FTS tests clearly shows the drastic difference in these bimetallic catalytic systems. The unpromoted iron catalyst and the FeZn catalyst show relatively higher initial catalytic activity, which quickly deactivate afterwards, while FeMn and FeCr catalysts exhibit a much lower initial catalytic activity but much better stability. This phenomenon is probably due to their difference in catalyst micro-structure resulted from variations in promoter types, which is categorized into two types according to their bimetallic interactions, namely (1) compound formation for FeZn catalyst and (2) solid solution formation for FeMn and FeCr catalysts. The difference from these two types of bimetallic interactions leads to their difference in catalyst physio-chemical properties and performance in FTS, such as surface area, extent of carburization, activity, selectivity, etc. Further study to correlate the catalyst structure changes with catalytic performance under industrial relevant conditions is needed to better understanding these promoted catalysts.

Acknowledgments

We thank the National Outstanding Young Scientists Foundation of China (20625620), the National Natural Science Foundation of China (20703054, 20590361) and the Innovation Funding Project of The Chinese Academy of Science (KJCX2-YW-N41). This work is also supported by Synfuels China. Co., Ltd. Special thanks to Dr. Zhi Xie and Prof. Shiqiang Wei (Beamline U7C) for help with EXAFS.

Appendix A. Supplementary data

Supplementary data associated with this article can be found, in the online version, at doi:10.1016/j.molcata.2010.04.009.

References

[1] R.B. Anderson, The Fischer–Tropsch Synthesis, Academic Press, Orlando, FL, 1984.
[2] M.E. Dry, The Fischer–Tropsch synthesis, in: J.R. Anderson, M.E. Boudart (Eds.), Catalysis—Science and Technology, Springer-Verlag, New York, 1981, p. 159.
[3] Y. Yang, H.W. Xiang, L. Tian, H. Wang, C.H. Zhang, Z.C. Tao, Y.Y. Xu, B. Zhong, Y.W. Li, Appl. Catal. A: Gen. 284 (2005) 105.
[4] H.J. Wan, B.S. Wu, T.Z. Li, Z.C. Tao, X. An, H.W. Xiang, Y.W. Li, J. Fuel Chem. Technol. 35 (2007) 589.
[5] Y. Yang, H.W. Xiang, Y.Y. Xu, L. Bai, Y.W. Li, Appl. Catal. A: Gen. 266 (2004) 181.
[6] C.H. Zhang, Y. Yang, B.T. Teng, T.Z. Li, H.Y. Zheng, H.W. Xiang, Y.W. Li, J. Catal. 237 (2006) 405.
[7] Y.M. Jin, A.K. Datye, J. Catal. 196 (2000) 8.
[8] S. Li, S. Krishnamoorthy, A.W. Li, G.D. Meitzner, E. Iglesia, J. Catal. 206 (2002) 202.
[9] S.D. Qin, C.H. Zhang, J. Xu, B.S. Wu, H.W. Xiang, Y.W. Li, J. Mol. Catal. A: Chem. 304 (2009) 128.
[10] G.C. Maiti, R. Malessa, M. Baerns, Appl. Catal. 5 (1983) 151.
[11] B. Kolk, A. Albers, Appl. Catal. 37 (1988) 57.
[12] L. Bai, H.W. Xiang, Y.W. Li, Y.Z. Han, B. Zhong, Fuel 81 (2002) 1577.
[13] R. Malessa, M. Baerns, Ind. Eng. Chem. Res. 27 (1988) 279.
[14] T.Z. Li, Y. Yang, C.H. Zhang, X. An, H.J. Wan, Z.C. Tao, H.W. Xiang, Y.W. Li, F. Yi, B.F. Xu, Fuel 86 (2007) 921.
[15] C.N. Satterfield, H.G. Stenger, Ind. Eng. Chem. Process Des. Dev. 23 (1984) 26.
[16] T.C. Bromfield, R. Visagie, U.S. Patent 049765A1 (2005).
[17] F. Domka, A. Basinska, R. Fiedovow, Surf. Technol. 18 (1983) 275.
[18] G.C. Chinchen, R.H. Logan, M.S. Spencer, Appl. Catal. 12 (1984) 69.
[19] S. Li, A. Li, S. Krishnamoorthy, E. Iglesia, Catal. Lett. 77 (2001) 197.
[20] S. Soled, E. Iglesia, S. Miseo, B.A. DeRites, R.A. Fiato, Top. Catal. 2 (1995) 193.
[21] Y.N. Yang, B. Zhong, S.Y. Peng, Q. Wang, J. Mol. Catal. (China) 7 (1993) 425.
[22] W.J. Zhong, B. He, Z. Li, S.Q. Wei, J. Univ. Sci. Technol. Chin. 31 (2001) 328.
[23] D.E. Sayers, B.A. Bunker, in: D.C. Koningsberger, R. Prins (Eds.), X-ray Absorption, Principles Applications, Techniques of EXAFS, SEXAFS and XANES, Wiley, 1988, p. 211.
[24] Y.Y. Ji, H.W. Xiang, Y.W. Li, Appl. Catal. A: Gen. 214 (2001) 77.
[25] T. Herranz, S. Rojas, M. Ojeda, F.J. Prez-Alonso, P. Terreros, K. Pirota, J.L.G. Fierro, Chem. Mater. 18 (2006) 2364.
[26] A.B. Gaspar, C.A.C. Perez, L.C. Dieguez, Appl. Surf. Sci. 252 (2005) 939.
[27] B. Liu, M. Terano, J. Mol. Catal. A 172 (2001) 227.
[28] A. Rahman, M.H. Mohamed, M. Ahmed, A.M. Aitani, Appl. Catal. A: Gen. 121 (1995) 203.
[29] R. Merryfield, M.P. McDaniel, G. Parks, J. Catal. 77 (1982) 348.
[30] M.J.N. Isfahania, M. Myndykb, V. Sepelak, J. Amighiana, J. Alloys Compd. 470 (2009) 434.
[31] F. Menil, J. Phys. Chem. Solids 46 (1985) 763.
[32] V. Sepelak, S. Wissman, K.D. Becker, J. Mater. Sci. 33 (1998) 2845.
[33] J. Zhao, Z. Fheng, F.E. Huggins, N. Shah, F. Lu, G.P. Huffmann, J. Catal. 143 (1993) 499.
[34] Y. Kou, B. Zhang, J. Niu, S. Li, H. Wang, T. Tanaka, S. Yoshida, J. Catal. 173 (1998) 399.
[35] A.N. Blacklocks, A. Atkinson, R.J. Packer, S.L.P. Savin, A.V. Chadwick, Solid State Ionics 177 (2006) 2939.
[36] S. Lee, P.R. Anderson, J. Colloid Interface Sci. 286 (2005) 82.
[37] E. Brauns, A. Rahme, H. Christmann, Arch. Eisenhuttenwesen 30 (1959) 553.
[38] M.G. Zhuravleva, G.I. Chufarov, D.Z. Brainina, Dokl. Akad. Nauk SSSR 132 (1960) 1074.
[39] M. Ding, Y. Yang, J. Xu, Z. Tao, H. Wang, H. Wang, H. Xiang, Y. Li, Appl. Catal. A: Gen. 345 (2008) 176.
[40] C.N. Satterfield, R.T. Hanlon, S.E. Tung, Z. Zou, G.C. Papaefthymiou, Ind. Eng. Chem. Prod. Res. Dev. 25 (1986) 407.
[41] W.S. Ning, N. Koizumi, H. Chang, T. Mochizuki, T. Itoh, M. Yamada, Appl. Catal. A: Gen. 312 (2006) 35.
[42] O.W. Perez-Lopez, A.C. Farias, N.R. Marcilio, J.M.C. Bueno, Mater. Res. Bull. 40 (2005) 2089.
[43] L. Xu, Q. Wang, D. Liang, X. Wang, L. Lin, W. Cui, Y. Xu, Appl. Catal. A: Gen. 173 (1998) 19.
[44] J. Zhao, Z. Fheng, F.E. Huggins, N. Shah, G.P. Huffmann, I. Wender, J. Catal. 148 (1994) 194.
[45] J. Zhao, Z. Fheng, F.E. Huggins, G.P. Huffmann, Energy Fuels 8 (1994) 38.
[46] F.J. Prez-Alonso, M. Lpez Granados, M. Ojeda, P. Terreros, S. Rojas, T. Herranz, J.L.G. Fierro, M. Gracia, J.R. Gancedo, Chem. Mater. 17 (2005) 2329.
[47] H. Kölbel, K.D. Tillmetz, U.S. Patent 4,177,203 (1979).
[48] C.K. Das, N.S. Das, D.P. Choudhury, G. Ravichandran, D.K. Chakrabarty, Appl. Catal. A: Gen. 111 (1994) 119.
[49] H. Zhao, D. Zhang, F. Wang, T. Wu, J. Gao, Process Saf. Environ. Protect. 86 (2008) 448.
[50] (a) R.M. Cornell, R. Giovaloni, Clay Clay Miner. 39 (1987) 11;
(b) R.M. Cornell, R. Giovaloni, Clay Clay Miner. 35 (1991) 144.
[51] (a) D.E. Janney, J.M. Cowley, P.R. Buseck, Am. Mineral. 85 (2000) 1180;
(b) D.E. Janney, J.M. Cowley, P.R. Buseck, Am. Mineral. 86 (2001) 327.
[52] J.L. Tambor, J.E. Dutrizac, Chem. Rev. 98 (1998) 2549.
[53] I.P. Saraswat, A.C. Vajpei, J. Mater. Sci. 15 (1980) 1326.
[54] J.K. Srivastava, K.G. Prasad, Phys. Status Solidi (B) 54 (1972) 755.
[55] K.B. Jensen, F.E. Massoth, J. Catal. 92 (1985) 98.
[56] G.J. Hutchings, J.C.A. Boeyens, J. Catal. 100 (1986) 507.
[57] Y.-F. Han, L.-W. Chen, K. Ramesh, Z.-Y. Zhong, F.-X. Chen, J.-H. Chin, H.-W. Mook, Catal. Today 131 (2008) 35.
[58] Y.-F. Han, F. Chen, Z.-Y. Zhong, K. Ramesh, E. Widjaja, L.-W. Chen, Catal. Commun. 7 (2006) 739.
[59] Y.-F. Han, F. Chen, Z.-Y. Zhong, K. Ramesh, L.-W. Chen, E. Widjaja, J. Phys. Chem. B 110 (2006) 24450.

[60] T. Birchall, A.F. Reid, J. Solid State Chem. 13 (1975) 351.
[61] G. Doppler, A.X. Trautwein, H.M. Ziethen, E. Ambach, R. Lehnert, M.J. Sprague, U. Gonser, Appl. Catal. 40 (1988) 119.
[62] M.D. Lee, J.F. Lee, C.S. Chang, Appl. Catal. 72 (1991) 267.
[63] F. Papa, L. Patron, O. Carp, C. Paraschiv, B. Ioan, J. Mol. Catal. A: Chem. 299 (2009) 93.
[64] H.L. Wang, Y. Yang, H. Wang, H.W. Xiang, Y.W. Li, J. Fuel Chem. Technol. (Chin.), accepted.
[65] T. Riedel, H. Schulz, G. Schaub, K.-W. Jun, J.-S. Hwang, K.-W. Lee, Top. Catal. 26 (2003) 41.
[66] T.R. Motjope, H.T. Dlamini, G.R. Hearne, N.J. Coville, Catal. Today 71 (2002) 335.
[67] L.D. Mansker, Y. Jin, D.B. Bukur, A.K. Datye, Appl. Catal. A: Gen. 186 (1999) 277.
[68] M. Ding, Y. Yang, B. Wu, J. Xu, C. Zhang, H. Xiang, Y. Li, J. Mol. Catal. A: Chem. 303 (2009) 65.
[69] S. Li, W. Ding, G.D. Meitzner, E. Iglesia, J. Phys. Chem. B 106 (2002) 85.
[70] J. Xu, C.H. Bartholomew, J. Phys. Chem. B 109 (2005) 2392.
[71] P.R. Dennison, K.J. Packer, M.S. Spencer, J. Chem. Soc., Faraday Trans. 85 (1989) 3537.
[72] M.S. Spencer, Catal. Lett. 50 (1998) 37.
[73] X.-M. Liu, G.Q. Lu, Z.-F. Yan, J. Beltramini, Ind. Eng. Chem. Res. 42 (2003) 6518.